On the crystallization of thin films composed of Sb3.6Te with Ge for rewritable data storage

Kooi, B. J.; De Hosson, J. Th. M.

Published in:
Journal of Applied Physics

DOI:
10.1063/1.1690112

Publication date:
2004

On the crystallization of thin films composed of $Sb_{3.6}Te$ with Ge for rewritable data storage

B. J. Kooi[a] and J. Th. M. De Hosson
Department of Applied Physics, Materials Science Center and Netherlands Institute for Metals Research, University of Groningen, Nijenborgh 4, 9747 AG Groningen, The Netherlands

(Received 20 November 2003; accepted 5 February 2004)

This article addresses the crystallization of amorphous $Sb_{3.6}Te$ films (40 nm thick) and 5 at. % Ge containing $Sb_{3.6}Te$ films (10, 20, and 40 nm thick) as studied with transmission electron microcopy using *in situ* annealing. These materials exhibit growth-dominated crystallization, in contrast to the usual $Ge_2Sb_2Te_5$ that shows nucleation-dominated crystallization. Particularly the crystal-growth velocity in these systems has been measured as a function of temperature from which the activation energy for growth can be derived. The strong effect of the 5 at. % Ge addition on the total crystallization behavior is revealed by the following four phenomena: Ge increases the crystallization temperature (from 95 to 150 °C), increases the activation energy for growth (from 1.58 to 2.37 eV), increases the nucleation rate and decreases the growth anisotropy. The crystallites have a special transrotational structure and a mechanism responsible for the development of this special structure is delineated. © *2004 American Institute of Physics.* [DOI: 10.1063/1.1690112]

I. INTRODUCTION

In phase change optical recording known from the rewritable CD and DVD formats, $Ge_2Sb_2Te_5$ is most widely used as the active medium for the rewritable information storage.[1–4] Amorphous areas embedded in a crystalline surrounding act as bits of information. A relatively high laser power is used to write these amorphous spots via a melt-quench process and medium and low laser powers are used for both erasing (crystallization) and reading, respectively. In particular the crystallization rate is becoming increasingly important because of the increasing demands on the data-transfer rates. Crystallization is the rate-limiting process, because amorphization is inherently a much faster process that in principle can be performed within femtoseconds.[5]

$Ge_2Sb_2Te_5$ shows nucleation-dominated crystallization, i.e., it nucleates easily and fast, but it shows only limited growth, with final sizes of the crystallites within a disk of 10–30 nm.[4,6] With the ongoing decrease of the amorphous-mark sizes due to a decrease in laser wavelength and an increase in numerical aperture of the focusing lens, phase-change materials showing very fast growth (i.e., growth-dominated crystallization) tend to become more preferable than $Ge_2Sb_2Te_5$, that is to say at least with respect to attainable data-transfer rates.[6,7] If the bit size decreases, the distance a fast growing crystal has to proceed from the edge of the amorphous mark to its center decreases and consequently the rewriting speed increases. For decreasing mark sizes, nucleation becomes less an issue since ''nuclei'' are always available near the edge of the mark. Therefore, phase-change materials showing very low nucleation rates, but fast growth rates become increasingly important. These kinds of materials are investigated in the present work. They are based on a Sb-rich Sb–Te eutectic composition ($Sb_{3.6}Te$), since it is known that these Sb-rich alloys show highest crystallization rates.[6] Also the strong effect of the addition of (5 at. %) Ge has been scrutinized.

The crystallization process is studied by transmission electron microscopy (TEM) using *in situ* heating. Advantage of this technique is that it provides detailed information with a high spatial resolution (nuclei with a size of 5 nm are easily detected), allowing nucleation (rates) and growth (rates) to be monitored separately. Most techniques for the determination of crystallization kinetics measure the overall crystallization rate, which is an interplay of nucleation and growth, but are unable to unravel these separate contributions. Crystal structure(s), crystal size distributions, crystal shapes, crystal orientations, and defects within the crystals grown can be assessed using TEM. A disadvantage of TEM could be that the electron beam of the TEM affects the crystallization process. In a previous study on $Ge_2Sb_2Te_5$ the electron beam turned out to strongly enhance the nucleation rate, obscuring a normal (isothermal or isochronal) analysis of the transformation kinetics.[8] This article will show that the situation for materials based on a Sb-rich Sb–Te eutectic composition is clearly more favorable, because crystallization is dominated by growth instead of by nucleation.

II. EXPERIMENT

Homogeneous master alloys of $Sb_{3.6}Te$ and of $Sb_{3.6}Te$ containing 5 at. % Ge were produced by mixing the pure components (Ge:6N, Sb, and Te, both 5N) in evacuated quartz tubes at 750 °C. Pieces of the ingot were positioned in pockets for electron beam evaporation. As substrates 10-nm-thick Si-nitride membranes were used. These transparent substrates were obtained by etching 100×100 μm^2 windows in a Si wafer containing the thin Si–nitride film on one side. A Varian electron beam evaporator with thickness monitor

[a]Author to whom all correspondence should be addressed; electronic mail: b.j.kooi@phys.rug.nl

was used for the deposition of 10-, 20-, and 40-nm thick amorphous films. Specimens were stored in vacuum to prevent oxidation of the films.

For TEM a JEOL 2010F operating at 200 kV was used. A Gatan double tilt heating holder (model 652 with a model 901 SmartSet hot stage controller) was used that employs a proportional integral differential controller for accurately control of the temperature (within ± 1 °C) and for a fast ramp rate to attain the desired final temperature without overshoot. Note that the temperature of the thin area that is imaged using TEM is generally lower than the nominal temperature indicated by the heating element within the specimen holder, i.e., the higher the temperature, the larger the discrepancy.

If during crystallization, nucleation and growth is monitored continuously using TEM, it is important to analyze the possible effects the electron beam of the TEM have on this nucleation and growth. This is possible, because the electron beam irradiates only a part of the sample during heating. In $Sb_{3.6}Te$ the incubation time for crystallization was observed to be about 5 min at 95 °C. At this temperature crystallization took place both within and outside the area exposed by the 200 kV electron beam of the TEM, although the nucleation rate was observed to be clearly higher within the electron-exposed area. At 85 °C, crystallization was in several cases observed to be complete within the electron-exposed area, whereas nucleation had not occurred at all in the much larger unexposed area. Since this showed that the nucleation rate of crystals is clearly affected by the electron beam of the TEM, it was also analyzed if the electron beam had any effect on the growth rate of the crystals. To this purpose crystals were nucleated at 95 °C after which the sample was cooled back to room temperature. At this temperature two nearly identical crystals were selected. After reheating to 95 °C one crystal was monitored during 10 min growth while subjected to electron-beam exposure whereas the other was outside the irradiated area. After cooling back to room temperature the size of the two crystals was compared. This procedure was repeated several times and it turned out that in general not significant differences in sizes (in growth speeds) between the two crystals could be observed, at least not more than the intrinsic variation in growth velocities for the different sessions. This showed that the electron beam does not affect the growth rate, it only increases the nucleation rate (particularly at the lowest possible crystallization temperatures). Of course the details in this behavior depend on the current density within the electron beam. Highest current densities that we applied were 3 nA in an exposed area with a diameter of about 2 μm. The smaller the current density the less the phase transformation is influenced, although it appears impossible to avoid effects on $Sb_{3.6}Te$ at 85 °C.

III. RESULTS

A. $Sb_{3.6}Te$

The isothermal growth of $Sb_{3.6}Te$ crystals in a 40-nm-thick amorphous film was monitored by *in situ* TEM in the temperature range 85–115 °C. Two problems had to be solved before growth rates of crystallization could be measured properly. We noted that the electron beam of the TEM, that irradiates a part of the sample during heating, clearly influenced the crystallization rate. Careful analysis, as elaborated in the experimental section, showed that the electron beam only increases the nucleation rate, i.e., most prominent at low temperatures just above the crystallization temperature T_c. Nonetheless, the electron beam does not noticeably affect the growth rate during crystallization. The second problem is related to the anisotropy in growth rates. This anisotropy is a logical consequence of the growth of single crystals where different crystallographic directions exhibit different growth rates. Fortunately, most crystals showed a strong preference to nucleate with the [0001] axis of the $R\bar{3}m$ structure perpendicular to the film surface. When observed plan-view these crystals have a triangular shape with often the $\{1\bar{1}20\}$ planes connecting the center of the triangle with the middle of the sides of the triangle. An example is shown in Fig. 1. The dark region at the bottom in each image is the Si wedge present at the edge of the Si–nitride window. Care was taken that, when measuring the growth rate at different temperatures, the same type of starting crystal was used as depicted in Fig. 1. To obtain these starting crystals, the 40-nm-thick amorphous $Sb_{3.6}Te$ film was heated for 5 min at 95 °C. Then after cooling to room temperature the correct starting crystals were searched for and their growth was subsequently monitored isothermally at 85, 95, 105, and 115 °C using *in situ* TEM. An example, showing a few of the bright-field TEM images recorded during the 85 °C growth, is presented in Fig. 1. Analysis of such a sequence of TEM images allows the determination of the size of the growing crystallite as a function of time. The result for all four temperatures is shown in Fig. 2. This graph clearly demonstrates

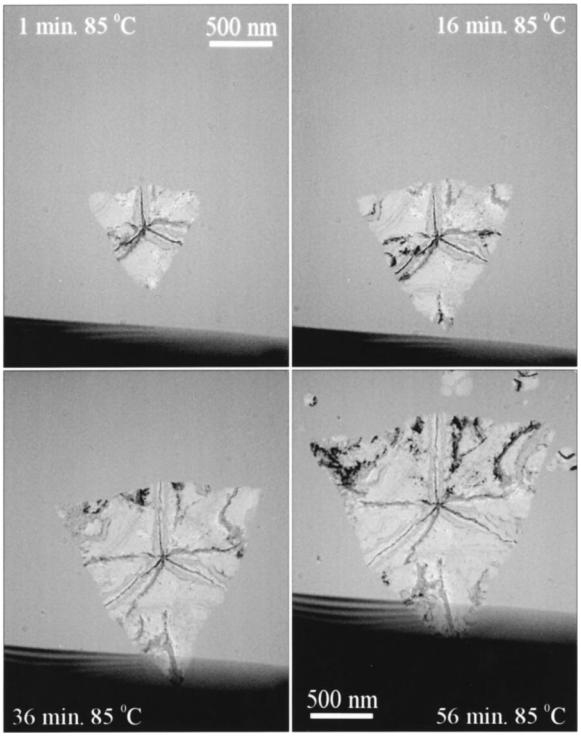

FIG. 1. Bright-field TEM images recorded during crystallization of a 40-nm-thick $Sb_{3.6}Te$ film at 85 °C. Note that the growing crystal was prenucleated by heating 5 min at 95 °C.

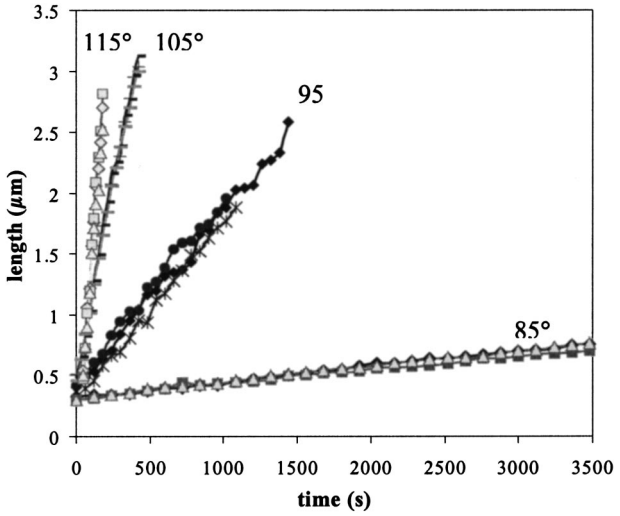

FIG. 2. Measured-crystallite sizes in 40-nm-thick $Sb_{3.6}Te$ as a function of annealing time at 85, 95, 105, and 115 °C.

that a very constant growth rate holds, i.e., the growth front of the crystal advances with a constant speed into the amorphous area. Such a constant growth rate generally implies an interface-controlled growth, in contrast to a diffusion-controlled growth. In the latter case the growth size depends usually on the square root of time. Using energy dispersive x-ray spectrometry (EDXS) in the TEM the composition on both sides of the amorphous-crystal interface was determined and no difference could be detected. Therefore, it is quite logical that interface-controlled growth occurs.

At 85 °C the interface velocity is about 0.12 nm/s, whereas at 115 °C it is 6.7 nm/s. So, the velocity is clearly temperature dependent and it is likely that an Arrhenius temperature dependence holds. Therefore, the logarithm of the growth velocity, i.e. the slope of the straight-line regressions in Fig. 2 is plotted as a function of the reciprocal temperature in Fig. 3. The slope of the linear fit to the data in Fig. 3 is directly related to Q_g/k, where Q_g is the activation energy

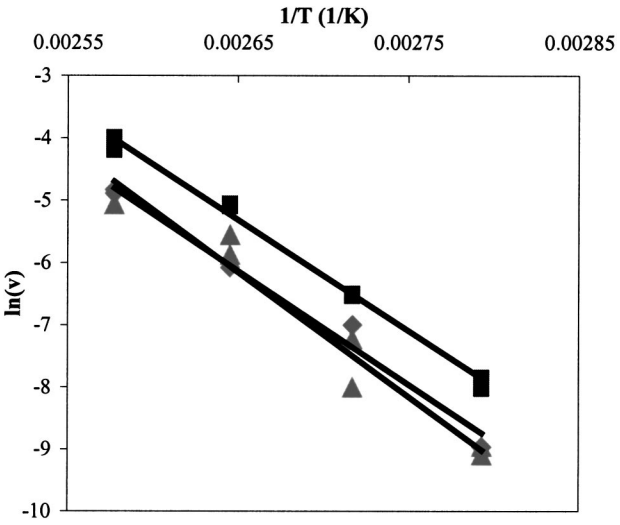

FIG. 3. Arrhenius plot showing the logarithm of the crystal growth velocity observed in 40-nm-thick $Sb_{3.6}Te$ vs the reciprocal temperature.

for growth and k is the Boltzmann's constant. The slope indicates an activation energy for growth of 1.58 ± 0.1 eV/atom (152 ± 10 kJ/mol). Note the higher velocities correspond to the square data points in Fig. 3. These velocities were obtained by measuring the distance between two corners along a side of the growing triangle and are thus for an equilateral triangle $\sqrt{3}$ higher than the real growth-front velocity. This measurement procedure was used, because it is the most accurate one and does not affect the slope of the straight-line regression in Fig. 3 and as a consequence gives the most accurate assessment of the activation energy for growth.

Although the electron beam to some extent affects the nucleation rate we can still draw a number of conclusions about the effect of the temperature on the nucleation rate. This is possible by analyzing at room temperature areas that during *in situ* heating were not exposed to the electron beam. From these observations it is clear that the nucleation rate strongly increases with temperature. An important characteristic is the final average grain size after isothermal crystallization as a function of temperature, because it shows the competition between nucleation and growth.[9] If the average grain size increases with increasing temperature then the activation energy for nucleation (Q_n) is smaller then the one for growth (Q_g) and if the average grains size decreases then $Q_n > Q_g$. Note that this only holds for a continuous nucleation rate. We observed that the typical grain size of about 4 μm did not change significantly as a function of temperature and therefore the activation energy for nucleation is likely to be similar to the one for growth.

In Fig. 4 a crystal grown after 12 min at 95 °C is shown in the central bright-field (BF) image together with four selected-area diffraction (SAED) patterns taken from four areas denoted by the circles 1–4 in the BF image. These SAED patterns indicate that the crystal can be assigned to the one of pure Sb, i.e., having the $R3m$ structure with $a = 0.43$ nm and $c = 1.13$ nm. Apparently the presence of almost 21 at. % substitutional Te in the Sb does not cause a significant change of the crystal structure of Sb. The SAED pattern 1, taken at the center of the triangular crystal where it nucleated, shows a 0001 zone axis pattern. The same pattern is present in the center of the triangular crystal in Fig. 1 and as mentioned earlier refers to the strong preference of a crystal to nucleate with the [0001] axis perpendicular to the film surface. The strong favor for this orientation can be understood since it corresponds to the one with the lowest surface energy of Sb.[10] Apart from a rotation of 120° around the viewing direction, SAED patterns 2–4 are identical and can be assigned as 1012 zone axes patterns. The angle between these $\langle 10\bar{1}2 \rangle$ directions and the central [0001] is 11.8°. Rotation of the sample in the TEM shows that the zone axes and the typical contrast features coming from the crystals in general move their position across the crystals. This typical contrast that is always present in all crystals corresponds to the well-known bend-contour contrast that can be observed quite usually in bent TEM foils. However, the crucial difference here is that the sample, i.e., the film itself does not have a bent shape, but remains flat. In contrast, the crystal planes inside the flat crystal are bent. The observations show that apparently during growth directly after nucleation a continu-

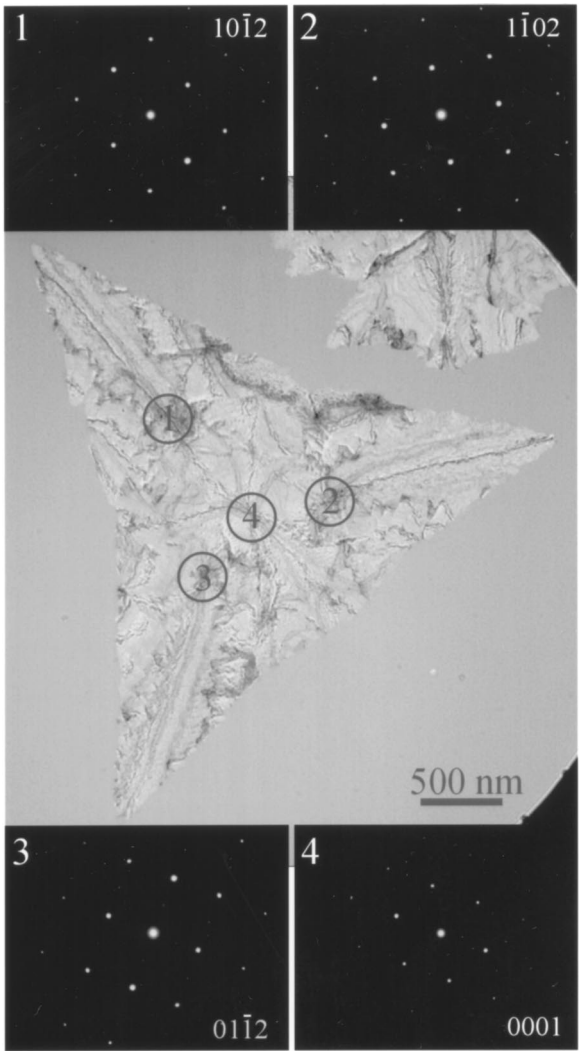

FIG. 4. Bright-field TEM image of a crystal grown after 12 min at 95 °C in a 40-nm-thick $Sb_{3.6}Te$ film together with selected area electron diffraction patterns of four areas indicated. It shows the general result that crystals nucleate with (0001) planes parallel to the surface after which during growth a continuous internal bending of the crystal planes occurs.

ous rotation of the crystal occurs during the lateral advance of the crystal. A schematic representation of a cross section through such a transrotational crystal is given in Fig. 5. It only shows the orientation of the (0001) planes. Typically, maximum tilts of about 25° are observed in the crystals. These tilts can be easily determined by rotating the sample until the central zone axis moves to the edge of the crystal. Also from tilting experiments in the TEM the sign of the curvature depicted in Fig. 5 is obtained. This sign of the curvature matters because the film is asymmetric with

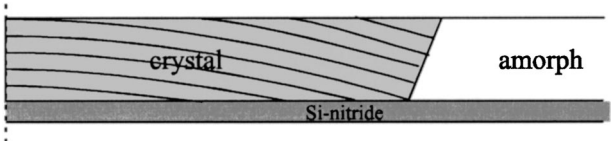

FIG. 5. Schematic cross section of a transrotational crystal that has grown in the amorphous film. Note the internal bending of the planes in a flat crystal. For clarity only the (0001) planes are indicated.

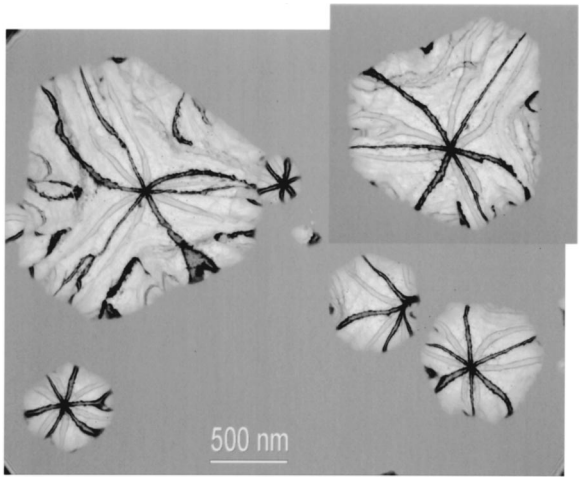

FIG. 6. Bright-field TEM image showing crystallites grown after 10 min at 155 °C in 40-nm-thick $Sb_{3.6}Te$ containing 5 at. % Ge.

vacuum on one side and the Si–N membrane on the other. We checked the sign of the curvature for many crystals and always found the same result. We also observed that the tilt per unit of lateral distance, grad ϕ, is highest for the smallest growth rates (i.e., at the lowest growth temperatures).

From the 0001 zone axis pattern with six-fold symmetry that is present in the center of the crystals it may appear contradictory that crystals with a triangular (three-fold symmetry) shape develop instead of with hexagonal shape. However, the $R3m$ structure, although described with hexagonal axes, corresponds to an $a-b-c$ stacking of the basal (0001) planes and not to a hexagonal $a-b$ stacking. In a crystal structure with hexagonal stacking the symmetry of the $[0\bar{0}01]$ axis is truly six-fold, but otherwise like here with the $R3m$ structure, because of the directions out of the (0001) plane it is three-fold. Therefore, due to the bending of the planes that occurs within the crystal, a true three-fold symmetry can arise.

B. $Sb_{3.6}Te$ with 5 at. % Ge

The isothermal crystallization of $Sb_{3.6}Te$ containing 5 at. % Ge for 10-, 20-, and 40-nm-thick films was monitored using *in situ* TEM in the temperature range between 140 and 170 °C. Compared to the previous section these higher temperatures were needed since the addition of Ge increased the crystallization temperature from about 95 to 150 °C.

At 155 °C the incubation time for crystallization in a 40-nm-thick film was observed to be about 5 min and after 10 min the crystals shown in the BF–TEM image of Fig. 6 had developed. Again, like in the previous section these crystals nucleate with the [0001] axis perpendicular to the film surface, but in contrast they do not show triangular shapes already for very small crystal sizes. Now, the small crystals are circular and the larger ones show hexagonal shape. Apparently the small amount of Ge suppresses the strong growth anisotropy present in $Sb_{3.6}Te$. Therefore, it was not needed to grow first starting crystals whose growth was subsequently monitored at the various temperatures. Again crystals with the peculiar transrotational structure develop. We

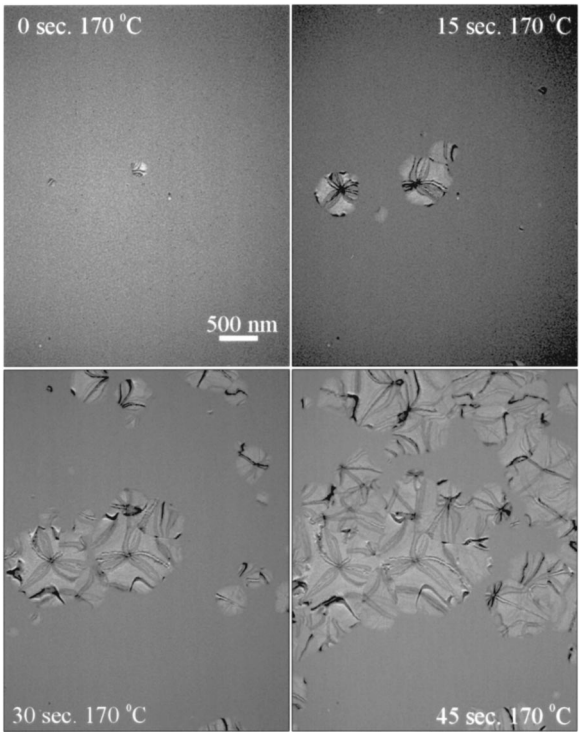

FIG. 7. Bright-field TEM images recorded during crystallization of a 40-nm-thick $Sb_{3.6}Te$ film containing 5 at. % Ge at 170 °C.

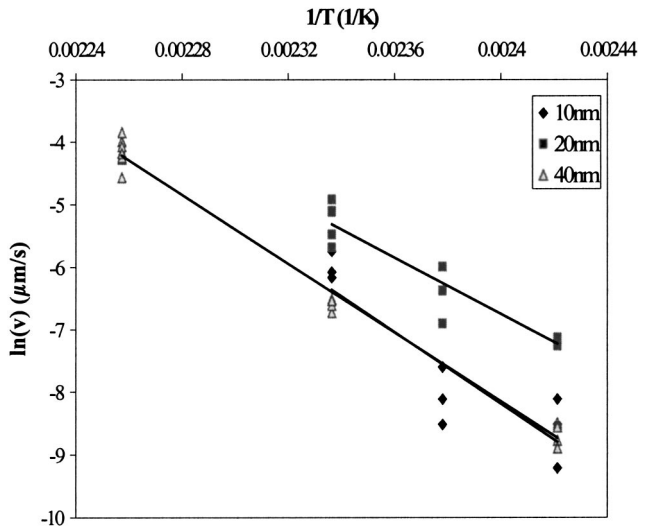

FIG. 8. Arrhenius plot showing the logarithm of the measured crystal-growth velocity vs the reciprocal temperature for $Sb_{3.6}Te$ with 5 at. % Ge for three film thickness' (10, 20, 40 nm).

measured that the tilt per unit of lateral distance, grad ϕ, is highest for the thinnest film (10 nm) and decreases with increasing film thickness (20 and 40 nm), i.e., about 70°/μm, 55°/μm, and 30°/μm for the 10-, 20-, and 40-nm-thick films crystallized at 155 °C. As in the previous section grad ϕ is highest for the lowest growth speeds.

An example, showing a few of the bright-field TEM images recorded during the 170 °C crystallization of a 40-nm-thick film, is given in Fig. 7. From these measurements the constant growth-front velocity was determined for various temperatures and for the three different film thickness after which the logarithm of the velocity is plotted as a function of the reciprocal temperature in Fig. 8. The results for the 40-nm-thick film show least scatter and lead to an activation energy of 2.37 ± 0.15 eV/atom (229 ± 15 kJ/mol). This can be directly compared with the 1.58 ± 0.1 eV of the previous section. It shows that the addition of Ge has increased the activation energy for growth with 50%. The growth velocities of $Sb_{3.6}Te$ with 5 at. % Ge in the temperature range between 140 and 165 °C are very similar to the ones observed for $Sb_{3.6}Te$ in the temperature range from 85 to 115 °C, namely from about 0.12 to 6.7 nm/s. The result of the 10-nm-thick film is, although showing more scatter, similar to the one of the 40-nm-thick film. However, for the 20-nm-thick film higher growth velocities, i.e., with a factor of 3–4 (when comparing the same temperatures) are observed, with lower activation energy of about 1.95 eV. To understand these deviations the precise compositions of the film are needed. The results of EDXS measurements of the composition of various film thicknesses are given in Table I. It shows that the film composition is not accurately reproduced during the different deposition sessions. This is an intrinsic problem using electron-beam evaporation of alloys. The 20 nm film deviates since it shows the lowest Ge (and Te and the highest Sb) concentration of the three films. Based on this low Ge concentration, it is logical that the 20 nm film shows a deviation towards the results obtained for ''pure'' $Sb_{3.6}Te$; i.e., a lower activation energy and due to the lower crystallization temperature a higher growth speed for a certain temperature (not far) above T_c. Following this reasoning the layer thickness itself does not affect the growth velocity during crystallization, but only the composition. On the other hand the final crystal size that develops after the transformation clearly depends on the film thickness. Figure 9 shows images obtained after 90 s crystallization at 155 °C for a 10 nm film in Fig. 9(a) and for a 20 nm film in Fig. 9(b). These images can be compared with the 10 min crystallization of the 40-nm-thick film shown in Fig. 6. Typical grain diameter that develops within the 10 nm film is 300 nm, within the 20 nm film 500 nm, and in the 40 nm film 1 μm. This 1 μm in the 40-nm-thick film is already clearly smaller than the 4 μm obtained in pure $Sb_{3.6}Te$ (when the same growth velocity holds). This allows us to draw the following conclusions: A strong increase in the nucleation rate compared to the growth rate is observed if Ge is added to $Sb_{3.6}Te$ or if the film thickness is reduced (from 40 to 10 nm). This increase in nucleation rate for decreasing film thickness seems a paradox. If nucleation occurs homogeneously throughout the material volume, then

TABLE I. Composition of the various films used for the present work as determined using EDXS coupled to the TEM.

	0 at. % Ge in $Sb_{3.6}Te$	5 at. % Ge in $Sb_{3.6}Te$	5 at. % Ge in $Sb_{3.6}Te$	5 at. % Ge in $Sb_{3.6}Te$
Film thickness	40 nm	10 nm	20 nm	40 nm
	at. %	at. %	at. %	at. %
Ge	⋯	4.5	3.8	5.0
Sb	78.3	74.0	76.4	74.4
Te	21.7	21.5	19.8	20.6

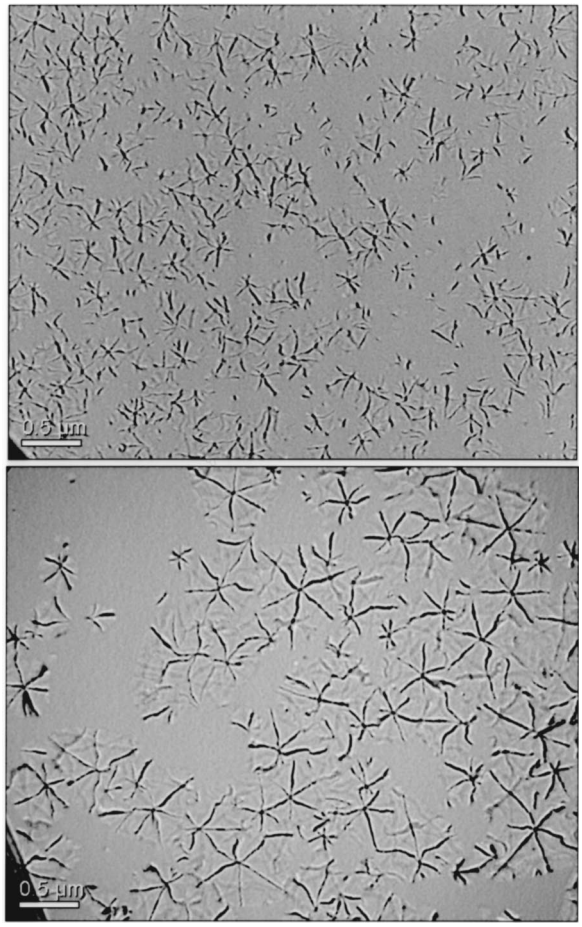

FIG. 9. Bright-field TEM images of $Sb_{3.6}Te$ with 5 at. % Ge after 90 s *in situ* heating in the TEM at 155 °C for (a) a 10-nm-thick and (b) a 20-nm-thick film.

the nucleation rate should decrease for decreasing film thickness. If nucleation occurs heterogeneously at the surface (or interface with the Si–nitride), then the nucleation rate is independent from the film thickness. Only if nucleation occurs by a mechanism where the interaction between the surface and the interface is important, then the nucleation rate could increase for decreasing film thickness. Apparently, this last case holds and nucleation is facilitated when the surface and interface approach each other. These results might be important for the explanation of the observed decrease in ''complete erasure time'' (CET) with decreasing film thickness for AgInSbTe alloys.[4,6,7] Although the present alloy is composed of Ge–Sb–Te its composition is such that is shows growth-dominated crystallization (as can be seen in the present results) like usually ascribed to AgInSbTe.[4,6] On the other hand $Ge_2Sb_2Te_5$ ($Ge_1Sb_2Te_4$ and $Ge_2Sb_4Te_7$), sometimes confusingly shortened to GeSbTe, shows nucleation-dominated crystallization, because growth of the crystallites hardly occurs with typical final sizes of 10–30 nm.[4,6] In these nucleation-dominated materials the CET increases for decreasing film thickness. The explanation for the decreasing CET with decreasing film thickness for growth-dominated materials can be found in the present results. It shows that the growth rate does not depend on film thickness, but that the nucleation rate increases for decreasing film thickness. In this way the overall crystallization rate increases for decreasing film thickness and therefore the CET decreases.

IV. DISCUSSION

A. Influence of Ge

The addition of about 5 at. % Ge in $Sb_{3.6}Te$ increased the crystallization temperature T_c from about 95 to 150 °C. We observed that the addition of 15 at. % Ge resulted in an increase to 220 °C. These increases in T_c are not surprising since compared to the Sb–Sb, Sb–Te, and Te–Te bonds the bonds involving Ge are clearly stronger (having more covalent character). The cohesive forces within the network predominantly determine the stability of a glass and thus the glass-transition temperature T_g.[11] Below T_g the structure is frozen and atomic rearrangement not possible leading to a stable amorphous structure. Crystallization can only occur above T_g and so T_g can serve as the lower limit for T_c. Indeed research has been devoted to the prediction of T_g in chalcogenide glasses[11–14] and recently T_g was predicted for the whole ternary Sb–Te–Ge ternary composition range.[11] T_g is then estimated as

$$T_g = x_{\mathrm{Ge}} T_g^{\mathrm{Ge}} + x_{\mathrm{Sb}} T_g^{\mathrm{Sb}} + x_{\mathrm{Te}} T_g^{\mathrm{Te}},$$
$$T_g(^\circ\mathrm{C}) = x_{\mathrm{Ge}} 525 + x_{\mathrm{Sb}} 147 + x_{\mathrm{Te}}(-69), \tag{1}$$

where x_i is the compositional fraction of element i in the alloy and T_g^i is the glass-transition temperature of the pure substance i. Using Eq. (1) T_g of $Sb_{3.6}Te$ with 0, 5, and 15 at. % Ge is predicted as 100, 121, and 164 °C, respectively. The predicted T_g of $Sb_{3.6}Te$ is slightly too high. The reason for this is that the calculated T_g of pure Sb as used in Eq. (1) is likely to be too high, because the calculation in Ref. 11 only considers covalent bonds whereas in Sb also some metallic bonding character is present.[11] On the other hand the effect of the addition of Ge is underestimated by the predictions. These underestimations may of course still be correct, since the predicted T_g should be a lower limit for T_c.

B. Transrotational crystals

The special structure of the transrotational crystals we observed was identified and studied in detail before,[15] but a proper explanation why this structure develops/exists is still lacking. Note that we adopted the term trans-rotational crystal as introduced by Kolosov *et al.*, because it appears to be a proper description of the peculiar structure; not a translational symmetry only, but to a specific translation also a specific rotation of the structure is connected. We present an explanation based on the increase in density that occurs upon the amorphous-crystalline phase transformation and it is visualized in the schematic cross section shown in Fig. 10. Of course it is a simplification of the actual transformation process, but still attempts to reproduce the key simplified steps responsible for the internal bending. For a thin film the increase in density particularly occurs perpendicular to the free surface, because only in this direction the shape change is unconstrained. Figure 10(a) shows that crystal planes that are initially horizontal, i.e., parallel to the surface outside the region where the densification of the structure occurs, grow

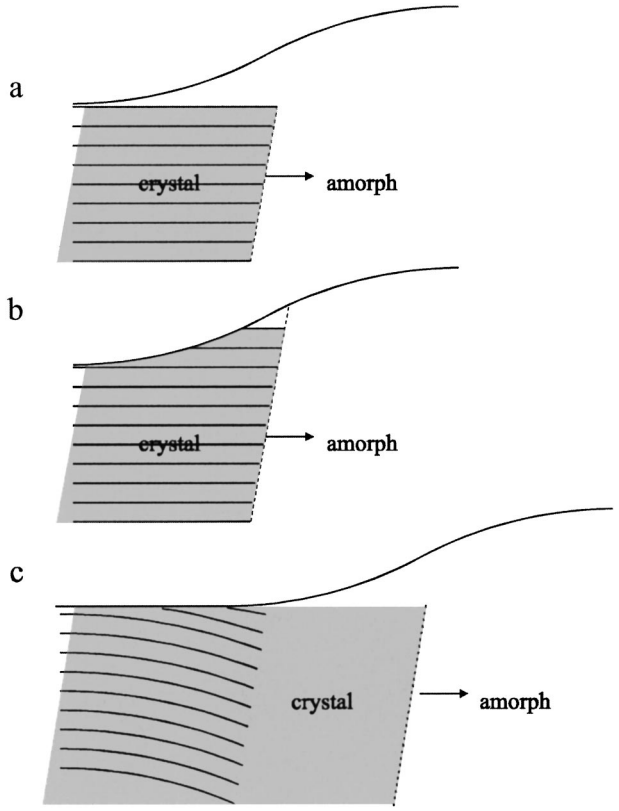

FIG. 10. Schematic illustration of the mechanism responsible for the internal crystal-plane bending present in transrotational crystals. First, crystal planes advance predominantly unbent into the amorphous matrix (a). Second, a (few) new crystal plane(s) nucleate(s) at the surface, where room is available, because due to the difference in specific volume the surface of the crystallite is at a lower height (level) than of the amorphous surrounding (b). Third, during further advance of the crystal/amorphous interface shrinkage associated with the transformation occurs causing a bending action on the advancing crystal planes (c).

more or less horizontally into the region where densification is not yet finished. This leaves room for nucleation of a (few) new crystal plane(s) in an amorphous area on top at the surface, because the surface of the amorphous region is higher than the one of the transformed (shrunk) crystalline region [Fig. 10(b)]. If the crystal front now proceeds into the amorphous area the shrinkage perpendicular to the surface occurs and causes bending of the already present crystal planes [Fig. 10(c)]. Note that this bending effect only occurs if the crystal front at the surface is ahead of the crystal front near the interface with the Si–nitride. Only in this way the crystal planes above can overgrow during bending the planes below. Because nucleation occurs at the film/vacuum interface and not at the film/Si–ntride interface,[8,16,17] it is also likely that this requirement holds. So, there is a tendency for bending of the crystal planes, but an additional requirement is that the material has to be sensitive to the bending action. This is also connected to the energetic stability of the internally bent structure.

In our opinion two factors make the material prone to bending: characteristic for the crystal structure is (1) its layered nature where generally a close-packed six-fold coordination holds within each layer and (2) its high vacancy concentration.[18,19] Bending of crystal planes is of course greatly facilitated if the bonding between adjacent planes is relatively weak, e.g., when dominated by van der Waals forces like in graphite. *Ab initio* electronic structure calculations have shown that rhombohedral $Ge_2Sb_2Te_5$ can indeed be considered as a layered structure with the presence of a weak bonding (low electron density) between the GeTe and TeSbTe layers.[20] Also, it is known that pure Sb can be considered as an $a-b-c$ stacking of close-packed planes. However, it has not an fcc crystal structure, because an alternating short and long distance is present between consecutive close-packed planes. Therefore, the structure is rhombohedral (with six close-packed planes stacked within the unit cell along the c axis). *Ab initio* electronic structure calculations have shown that indeed alternating stronger and weaker bonding is present between close-packed planes.[21,22] In this respect the following statements in Ref. 22 are of interest: ''This stacking of pairs of planes (along the trigonal axis) can explain the easy cleavage properties of this type of monocrystals. The anisotropy of these crystals is, however, less obvious than for other two-dimensional materials, such as graphite.'' The present $R\bar{3}m$ structure of $Sb_{3.6}Te$ (with 0 and 5 at. % Ge) is isomorph with the crystal structure of pure Sb and also shows a similar layered structure as rhombohedral $Ge_2Sb_2Te_5$. The conclusion is therefore clear that these materials have a layered structure facilitating bending.

We expect that the relative high vacancy concentration in these materials results in a further facilitation of bending. To give some rationalization to this expectation, the following consideration can be given. For a flat graphite sheet it is known that if the hexagon is locally replaced by a single pentagon a 60° disclination is introduced.[23] In the same manner an ordered structure of pentagons surrounded by hexagons result in the well-known curved structures present in fullerenes. This illustrates the fact that based on a flat layered structure, the presence of a vacancy can give rise to a rotational distortions. Particularly if the six-fold coordination due to a vacancy (during growth) leads to a *locally relaxed* structure with five-fold coordination. Of course, the close-packed plane in the phase-change materials are not built out of hexagons, but still the high vacancy concentration present leads to a closer resemblance with graphite sheets.

For the transrotational α-Fe_2O_3 crystals formed during the (electron-beam) crystallization of iron–oxide, it was also observed that the tilt per distance is highest for the lowest growth speeds.[15] The explanation for this observation is, as based on the mechanism proposed in Fig. 10, relatively straightforward. For bending it is essential that new planes nucleate at the surface in the region above the horizontally advancing crystal planes [cf. Fig. 10(b)]. This region is present because the surface of the amorphous region is higher than of the shrunk crystalline one. If as a function of time the same total number of new planes can initiate at the surface (which is most logical assumption, because nucleation is predominantly a statistical process with time) then their density as a function of lateral distance is directly proportional to the growth velocity. The higher the growth speed the lower the density of newly initiated crystal planes at the surface and the lower the tilt per unit of lateral distance, grad ϕ. The maximum grad ϕ is, according to this physical

picture, related to the ratio between the height difference of the crystalline-amorphous area and the (minimum) lateral width where this transition in height occurs. So, the larger the increase in relative density upon the transformation and the smaller the interface width (related to the elastic constants of the material) the larger the maximum possible grad ϕ.

Although experimental results for various film thickness t were not shown in Ref. 15, they stated that based on simple elastic considerations the maximum strain in the film $\epsilon = (t/2)\text{grad}\,\phi$. Therefore, the elastic strain increases for increasing film thickness making bending less favorable for thicker films. Although the actual strain in the films does not have to be purely elastic, it will still be the dominant effect explaining the decrease of grad ϕ for increasing film thickness we observe.

V. CONCLUSIONS

This article shows that *in situ* TEM is a versatile tool to study crystallization of amorphous thin films. Here, results for the crystallization of $Sb_{3.6}Te$ films (40 nm thick) and 5 at. % Ge containing $Sb_{3.6}Te$ films (10, 20, and 40 nm thick) are shown. The measured growth-front velocities vary between 0.12 and 6.7 nm/s in the temperature range 85–115 °C for $Sb_{3.6}Te$ and in the range 140–165 °C for 5 at. % Ge containing $Sb_{3.6}Te$. The important effect of the 5 at. % Ge addition on the crystallization behavior is revealed, namely: Ge increases the crystallization temperature (from 95 to 150 °C), increases the activation energy for growth (from 1.58 to 2.37 eV), increases the nucleation rate and decreases the growth anisotropy. The nucleation rate of these materials showing growth-dominated crystallization also increases with decreasing film thickness. Crystals that grow have a peculiar transrotational structure. A mechanism is presented that explains why this structure arises and in particular it is capable of explaining observed dependence of the transrotational structure on growth speed and film thickness.

ACKNOWLEDGMENT

Thanks are due to W. M. G. Groot for some of the *in situ* TEM experiments.

[1] N. Yamada, E. Ohno, K. Nishiuchi, and N. Akahira, Jpn. J. Appl. Phys., Suppl. **26**, 61 (1987).
[2] K. Nishimura, M. Suzuki, I. Morimoto, and K. Mori, Jpn. J. Appl. Phys., Suppl. **28**, 135 (1989).
[3] H. J. Borg and R. van Woudenberg, J. Magn. Magn. Mater. **193**, 519 (1999).
[4] G.-F. Zhou, Mater. Sci. Eng., A **304–306**, 73 (2001).
[5] T. Ohta, N. Yamada, H. Yamamoto, T. Mitsuyu, T. Kozaki, J. Qiu, and K. Hirao, Mater. Res. Soc. Symp. Proc. **674**, V1.1.1 (2001).
[6] H. Borg, M. Lankhorst, E. Meinders, and W. Leibrandt, Mater. Res. Soc. Symp. Proc. **674**, V1.2.1 (2001).
[7] H. J. Borg, P. W. M. Blom, B. J. A. Jacobs, B. Tieke, A. E. Wilson, I. P. D. Ubbens, and G. Zhou, Proc. SPIE **3864**, 191 (1999).
[8] B. J. Kooi, W. M. G. Groot, and J. Th. M. De Hosson, J. Appl. Phys. **95**, 924 (2003).
[9] G. Ruitenberg, A. K. Petford-Long, and R. C. Doole, J. Appl. Phys. **92**, 3116 (2002).
[10] A. K. Petford-Long, R. C. Doole, C. N. Alfonso, and J. Solis, J. Appl. Phys. **77**, 607 (1995).
[11] M. H. R. Lankhorst, J. Non-Cryst. Solids **297**, 210 (2002).
[12] J. P. deNeufville and H. K. Rockstad, in Proc. 5th Int. Conf. Amorphous and Liquid Semiconductors, edited by J. Stuke and W. Brenig, 1974, p. 419.
[13] M. Lasocka, Z. Phys. Chem., Neue Folge **156**, 123 (1988).
[14] L. Tichy and H. Ticha, J. Non-Cryst. Solids **189**, 141 (1995).
[15] V. Yu. Kolosov and A. R. Thölen, Acta Mater. **48**, 1829 (2000).
[16] T. H. Jeong, M. R. Kim, H. Seo, S. J. Kim, and S. Y. Kim, J. Appl. Phys. **86**, 774 (1999).
[17] N. Ohshima, J. Appl. Phys. **79**, 8357 (1996).
[18] J. M. Yanez-Limon, J. Gonzalez-Hernandez, J. J. Alvarado-Gil, I. Delgadillo, and H. Vargas, Phys. Rev. B **52**, 16321 (1995).
[19] A. Mendoza-Galvan and J. Gonzalez-Hernandez, J. Appl. Phys. **87**, 760 (2000).
[20] S. Yamanaka, S. Ogawa, I. Morimoto, and Y. Ueshima, Jpn. J. Appl. Phys., Part 1 **37**, 3327 (1998).
[21] L. F. Mattheiss, D. R. Hamann, and W. Weber, Phys. Rev. B **34**, 2190 (1986).
[22] X. Gonze, J.-P. Michenaud, and J.-P. Vigneron, Phys. Rev. B **41**, 11827 (1990).
[23] A. Krishnan, E. Dujardin, M. M. J. Treacy, J. Hugdahl, S. Lynum, and T. W. Ebbensen, Nature (London) **388**, 451 (1997).